

Oxidation of C₅ esters: Influence of the position of the ester function

Guillaume Dayma^{1,2}, Sébastien Thion¹, Maxence Lailliau¹, Zeynep Serinyel^{1,2}, Philippe
Dagaut¹

¹CNRS-INSIS, 1C, Ave de la recherche scientifique – 45071 Orléans cedex 2, France

²Université d'Orléans, 1 rue de Chartres – BP 6759 – 45067 Orléans cedex 2, France

Corresponding author: guillaume.dayma@cnrs-orleans.fr

Phone: (+33) 238 255499

fax: (+33) 238 696004

Keywords: oxidation, jet-stirred reactor, kinetic modeling, methyl butanoate, ethyl propanoate, propyl acetate, butyl formate

Abstract

The oxidation of esters has been extensively studied over the last 15 years, mainly focusing on methyl- and ethyl-esters. Recently, the oxidation of esters produced from higher alcohols has received more and more attention. In this work, we report experiments and modeling on the oxidation of a series of four esters with five carbon atoms, namely, methyl butanoate, ethyl propanoate, propyl acetate, and butyl formate. The oxidation of these esters was performed in a jet-stirred reactor under the same experimental conditions ($\tau = 700$ ms, $p = 10$ atm, $\phi = 1$, and $X_{\text{fuel, initial}} = 1000$ ppm). The mole fraction profiles obtained from these experiments were used to develop a unique detailed kinetic mechanism for the oxidation of these four esters, which performs well against our experimental data and on data from the literature. Although these esters are isomers, this work highlights the influence of the position of the ester function in terms of global reactivity and product distribution. In particular, this comparison shows the

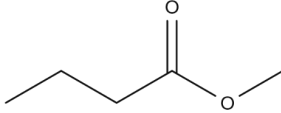
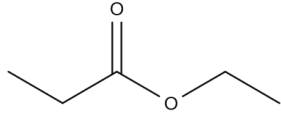
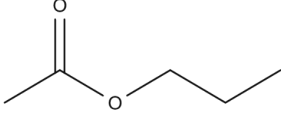
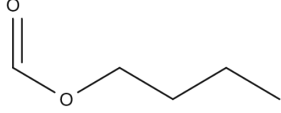
strong impact of the nature of the products (i.e. acid + alkene) formed by the different molecular decomposition reactions during the oxidation process of these esters.

1. Introduction

Biodiesel has been the subject of several studies since the end of the 20th century. Starting with the pioneer works on methyl acetate ¹ or methyl butanoate ², recent studies focused on esters with longer acid chains ³, unsaturations ^{4,5} or longer alcohol chains ^{6,7}. Biodiesel is considered as an interesting alternative to petroleum derived Diesel fuel in order to mitigate the increasing demand on oil products for transportation. It also offers an opportunity to limit CO₂ emissions in the atmosphere by a short carbon cycle: from CO₂ emitted during the combustion of the plant by-products to the use of this CO₂ for the plant to grow. Indeed, biodiesel is composed of monoalkyl esters of long carbon chain fatty acids obtained from the transesterification of renewable lipid feedstock with mostly methanol, but also ethanol or higher molecular weight alcohols.

With the growing interest on higher alcohols ⁸⁻¹³, esters with higher energy content can be produced and burned in engines for ground transportation, especially Diesel engines ^{14,15}. Therefore, this paper focuses on the influence of the position of the ester function along the carbon chain, as depicted in Table 1, and highlights the importance of the nature of the products formed by the different molecular reactions in terms of global reactivity or product distribution. Experiments performed in a jet-stirred reactor under the same conditions ($\tau = 700$ ms, $p = 10$ atm, $\phi = 1$, and $X_{\text{fuel, initial}} = 1000$ ppm) with methyl butanoate, ethyl propanoate ¹⁶, propyl acetate ¹⁷, and butyl formate ⁷ were compiled and reexamined in order to point out how the position of the ester function can modify the reactivity of these compounds.

Table 1. Chemical structure of C₅ esters, heat of formation (kcal mol⁻¹) and entropy (cal mol⁻¹ K⁻¹) @ 298 K.

Species		$\Delta_f H^\circ$	S°	Ref.
Methyl butanoate - MB		-107.70	93.69	18
Ethyl propanoate - EP		-111.00	94.17	16
Propyl acetate - PA		-111.00	95.65	17
Butyl formate - BF		-102.71	99.47	7

2. Experimental

A series of experiments was performed over several years in the same jet-stirred reactor that has been described in detail earlier^{19,20}. Briefly, the reactor itself is a fused-silica sphere (38 cm³) with four nozzles. A perfect stirring is obtained thanks to the high turbulent jets formed at the exit of the thin nozzles. The reactants were diluted with nitrogen (<100 ppm H₂O, <50 ppm O₂, <1000 ppm Ar, <5 ppm H₂ from Air Liquide) and preheated. They mixed at the entrance of the injectors to avoid reactions prior to the reactor. In each case, a high-degree of dilution (1000 ppm mol. of fuel) was used to limit temperature gradients inside the reactor. The reactants were oxygen (99.995% pure from Air Liquide) and methyl butanoate (99% pure from Aldrich, CAS 623-42-7), ethyl propanoate¹⁶, propyl acetate¹⁷, and butyl formate⁷. An HPLC pump (Shimadzu LC10 AD VP) with an on-line degasser (Shimadzu DGU-20 A3) was used to deliver the fuel to an atomizer-vaporizer assembly maintained at 120 °C. A good thermal

homogeneity (gradients < 1 K/cm) was checked along the vertical axis of the reactor by thermocouple measurements (0.1 mm Pt-Pt/Rh-10%) for each experiment. The thermocouple is located inside a thin-wall fused silica tube to prevent catalytic reactions on the metallic wires. For each selected temperature, the reacting mixture was sampled using a fused-silica low-pressure sonic probe. Samples flowed to analyzers or bulbs via a Teflon heated line maintained at 140 °C. Online analyses were performed using a Thermo Nexus 670 Fourier Transformed IR spectrometer (10 m path length, resolution of 0.5 cm^{-1} , 200 mbar in the cell). After collection and storage at low pressure (50 mbar) in 1 L Pyrex bulbs, off-line analyses were performed using gas chromatographs (GC) equipped with capillary columns (0.32 mm i.d. DB-624, 0.32 mm i.d. CP-Al₂O₃-KCl, 0.53 mm i.d. CP-Carboplot-P7, 0.32 mm i.d. CP-SIL 5CB coupled to 0.53 mm i.d. DB1-MS), a TCD (thermal conductivity detector), and a FID (flame ionization detector). Two GC-MS (Varian CP3800-V1200 and Shimadzu GC-MS 2010 Plus) operating with electron impact ionization (70 eV) were used for identification.

Methyl butanoate has already been studied in this JSR ¹⁸, but under different experimental conditions. Therefore, experiments with methyl butanoate as fuel were performed under the same conditions as its other three isomers. The experiments were performed at steady state, at a constant mean residence time, τ , of 0.7 s. Reactants continually flowed through the reactor, while the temperature of the gases inside the JSR was increased stepwise. A good repeatability of the analysis for each experiment and a reasonably good carbon balance (typically $100 \pm 10\%$) were achieved in these four different experiments over the years.

3. Kinetic modeling

The chemical kinetic modeling in JSR for the four isomers was performed using the PSR code ²¹ from CHEMKIN II. The input files for each simulation include a unique detailed chemical kinetic mechanism, and a dataset of thermochemical properties. Mechanism,

thermodynamic data as well as experimental data are available as supplemental material to this publication or directly from the authors.

The kinetic reaction mechanism in this study was extended from the scheme proposed for the oxidation of butyl formate and small hydrocarbons in a JSR at high-pressure^{7,22,23}. It was developed including the submechanisms previously proposed for methyl butanoate¹⁸, ethyl propanoate¹⁶, and propyl acetate¹⁷ oxidation. Thermochemical properties were also taken from our previous studies. Rate rules for H-abstraction and β -scission reactions in all these submechanisms were homogenized according to our previous works in order to obtain a full self-consistent mechanism. The use of the same rate parameters for each of these isomers is supported by the bond dissociation energies taken from²⁴ for MB and EP, from¹⁷ for PA, and⁷ for BF and summarized in Table 2. The full version of the proposed mechanism consists of 628 species reacting in 3929 reactions.

Table 2: BDEs for C–H, C–C (bold, italic), and C–O (italic, underlined) bonds taken from²⁴ for MB and EP, from¹⁷ for PA, and⁷ for BF at 298 K.

<p>MB</p>	<p>EP</p>
<p>PA</p>	<p>BF</p>

4. Results and Discussion

4.1 Fuel reactivity

The experiments were conducted under the same conditions: constant mean residence time of 0.7 seconds, constant pressure of 10 atm, stoichiometric mixtures ($\varphi = 1$), and 1000 ppm as an initial fuel mole fraction. Common species were detected during the oxidation the 4 isomers (H_2 , H_2O , CO , CO_2 , CH_2O , CH_4 , C_2H_4 , C_2H_6 , C_2H_2 , C_3H_6 , CH_3CHO) whereas some others were fuel-specific (formic acid, acetic acid, propanoic acid, butanal, propanal, or 1-butene and acrolein).

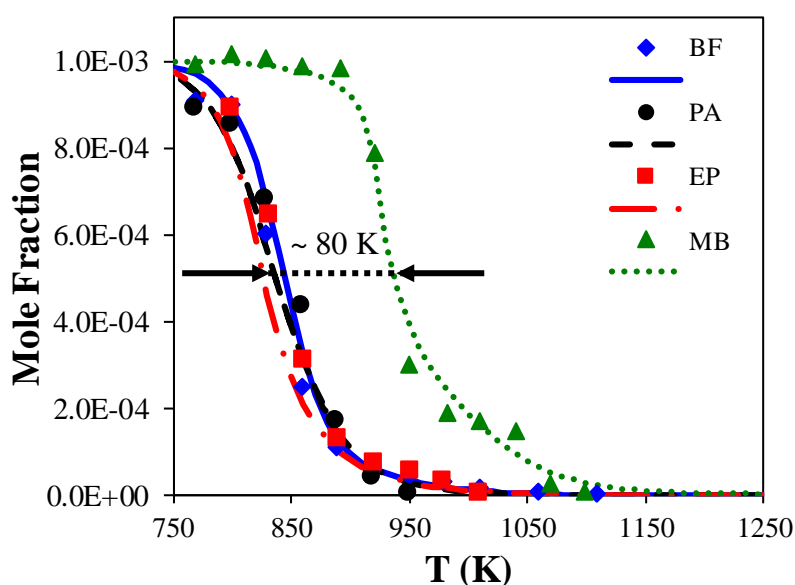
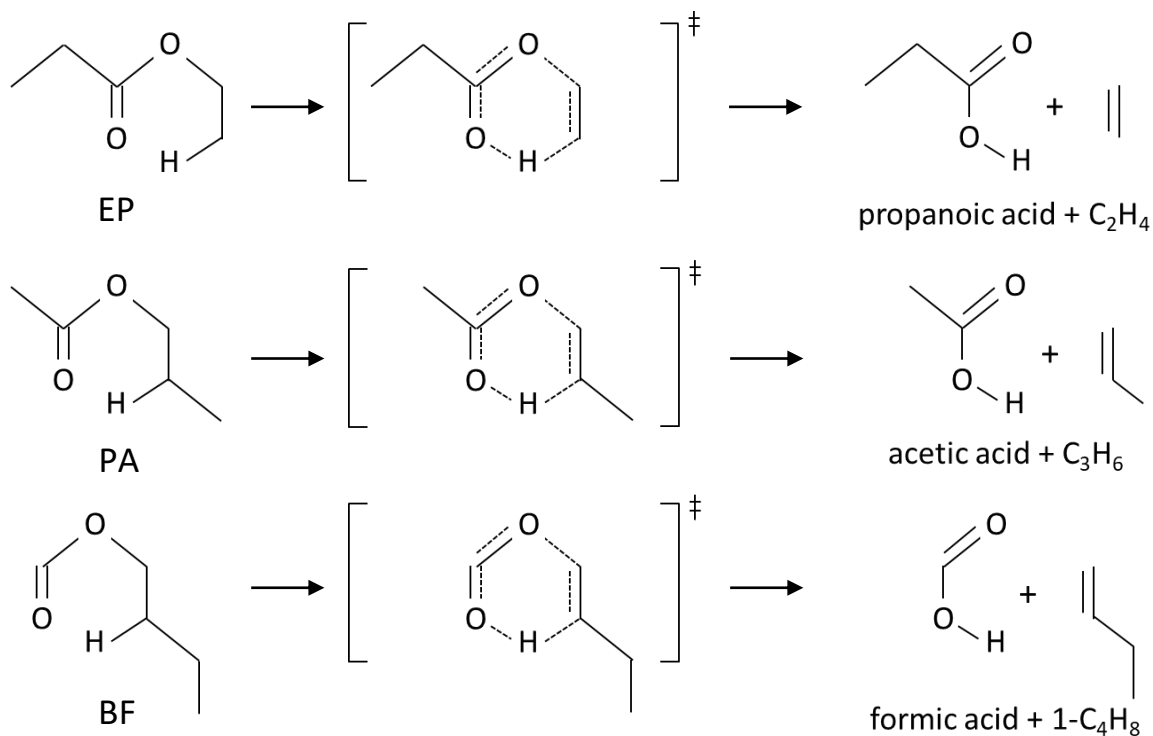


Figure 1: Experimental (large symbols) and computed (lines) mole fraction profiles obtained from the oxidation of methyl butanoate (green), ethyl propanoate (red), propyl acetate (black), and butyl formate (blue) in a JSR at $\varphi = 1$, $p = 10$ atm, $\tau = 0.7$ s.

Figure 1 shows the evolution of the mole fraction of the four different isomers as a function of the temperature. It can be seen from this figure that butyl formate (BF), propyl acetate (PA), and ethyl propanoate (EP) have very a similar conversion while methyl butanoate (MB) reacts at higher temperatures. Half of BF, PA, and EP is consumed ca. 80 K before MB. The basic difference between MB, and the other three lies in the possibility for BF, PA, and EP

to react via a six-membered ring molecular decomposition reaction, such as illustrated in Table 3.

Table 3: Schematic overview of the six-membered ring molecular decomposition reaction.



Following this pathway, BF yields formic acid and 1-butene, PA, acetic acid and propene, and EP, propanoic acid and ethylene. Reaction pathway analyses were performed at 870 K in all four cases, temperature at which 70-80% of BF, PA, and EP are consumed whereas only 5% of MB has reacted. Under these conditions, according to our detailed kinetic mechanism, 40% of BF gives 1-butene and formic acid through the molecular elimination, and 54% is consumed by H-abstraction reactions, mostly by OH, yielding five possible radicals. This reaction pathway analysis is very similar for EP, 36% of which is consumed by the molecular elimination yielding ethylene and propanoic acid, and 60% by H-abstraction reactions, again mostly by OH, producing four radicals. However, in the case of PA, the reaction pathway analysis reveals this compound is exclusively consumed by the molecular

elimination giving propene and acetic acid, H-abstraction reactions playing virtually no role in the consumption of PA, whereas PA is clearly as much consumed as BF or EP. On the contrary, MB, which is far less consumed at this temperature, reacts exclusively through H-abstraction reactions, mostly with OH and CH₃, and gives four primary radicals. Thus, despite their close reactivity, differences are observed in the reaction pathways between BF and EP on one hand, and PA on the other hand. These differences cannot be explained by differences in the rate constants of the molecular reactions used in the kinetic mechanism because they are indeed very close, as can be seen in Fig. 2, proceeding through a similar six-membered ring transition state as mentioned above. The rate constant of this molecular reaction was recently determined experimentally and theoretically for PA¹⁷, whereas it was estimated by Dayma et al.²⁵ for EP, and theoretically calculated by Zaras et al.⁷ for BF.

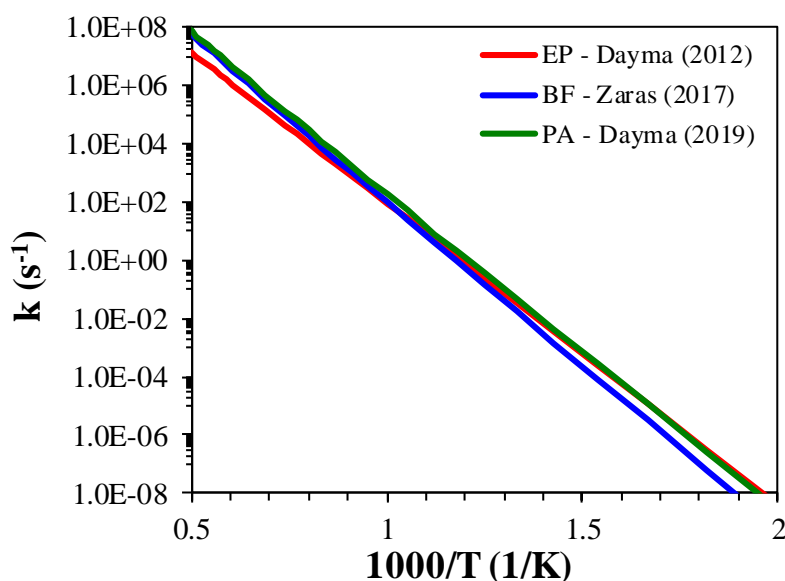


Figure 2: Rate constants of the molecular reactions for ethyl propanoate (EP)²⁵, butyl formate (BF)⁷, and propyl acetate (PA)¹⁷.

Thus, the difference in the reaction pathways between butyl formate and ethyl propanoate on one hand and propyl acetate on the other hand should come from the radical

pool. Rates of production (ROP) of OH radicals were also computed for the four esters under the same conditions. OH ROP was found to be: 2.26×10^{-7} mol cm⁻³ s⁻¹ for BF, 2.83×10^{-7} mol cm⁻³ s⁻¹ for EP, while only 4.68×10^{-10} mol cm⁻³ s⁻¹ for PA, i.e. 480 times lower than BF and 600 times lower than EP, and 3.65×10^{-9} mol cm⁻³ s⁻¹ for MB. Looking deeper into the reaction pathway analysis at 870 K, it turns out that, for EP and BF, OH is mostly produced from the decomposition of H₂O₂ (75 % in EP and 61 % in BF) and from CH₃ + HO₂ reaction to a lesser extent (11 % in both EP and BF). H₂O₂ comes from HO₂, mostly from the reaction with itself, while HO₂ formation proceeds through 3 major pathways: H + O₂ + M, C₂H₅ + O₂, and HCO + O₂, with reaction rates not significantly different between EP and BF. In the case of MB, though much less produced, routes of formation of OH are basically the same via H₂O₂ and HO₂. The major difference is that C₂H₅ is much less involved in the production of HO₂ in that case, HO₂ being mostly produced by H + O₂ + M (47 %), MB2j + O₂ (25 %), and HCO + O₂ (15 %). The formation of methyl-2-butenate from MB2j replaces C₂H₅ in this case. Finally, for PA, things are rather different. First of all, OH is far less produced, but also the routes leading to OH are different. More than 60 % of OH comes from propene (produced by the molecular decomposition reaction), allyl and subsequent reactions, c.a. 9 % from CH₃ + HO₂, and only 29 % from H₂O₂ decomposition. C₂H₅ is not involved in the formation of OH in the latter case, and this absence of ethyl radicals seems to be responsible for the very limited production of OH. Therefore, looking further into the reactions involved in the production or the consumption of ethyl radicals, it appears that, in the case of BF, EP, and MB to a lesser extent, an interesting loop is taking place between C₂H₅ and C₂H₄, recycling C₂H₅ from C₂H₄ and producing HO₂, in turn, which is responsible for the formation of OH, and hence the consumption of the fuels. This loop is presented in Fig. 3 a-c for EP, BF, and MB respectively with the rates of production (in mol cm⁻³ s⁻¹) of each route. It can be seen from this figure that C₂H₅ is oxidized by O₂ and produces C₂H₄ either directly or through the intermediate C₂H₅O₂,

yielding HO₂ from both channels. A significant part of C₂H₄ is then recycled into C₂H₅ by C₂H₄ + H ⇌ C₂H₅, enhancing the production of OH. In the case of PA, this loop is broken because C₂H₅ is not recycled from C₂H₄, but indeed produces C₂H₄. This equilibrium is reversed, probably because of the very low C₂H₄ concentration, resulting from a lack of global reactivity, because the loop between C₂H₅ and C₂H₄ is broken. Unfortunately, when such loops appear in stationary reactors (as a PSR), it is not possible to go further in the analysis: a study in a time-dependent reactor might help solving this issue of the influence of the loop between C₂H₅ and C₂H₄.

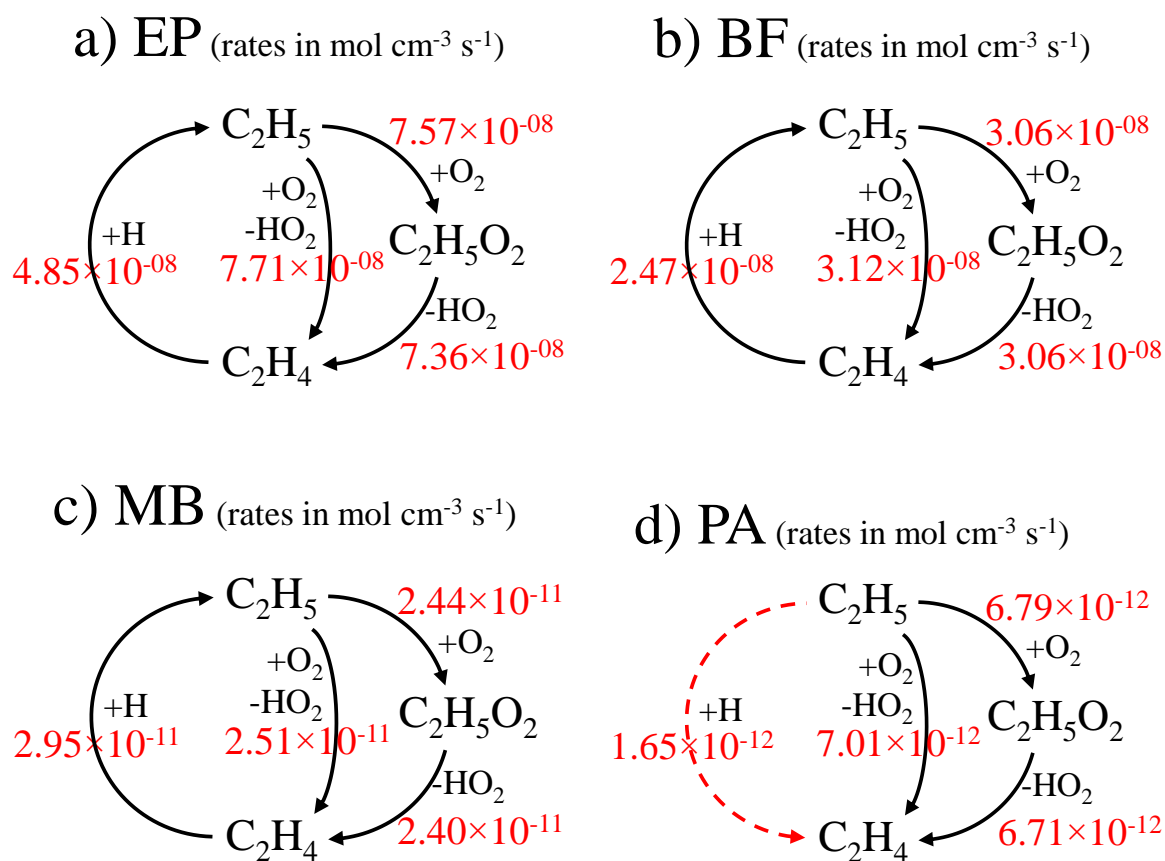


Figure 3: Rates of consumption and formation (mol cm⁻³ s⁻¹) of C₂H₅ calculated at $T = 870$ K, $p = 10$ atm, $\varphi = 1$, and $\tau = 0.7$ s for a) ethyl propanoate (EP), b) butyl formate (BF), c) methyl butanoate (MB), and d) propyl acetate (PA).

4.2 Intermediates and products

Figure 4 shows the evolution of H₂O and CO₂ mole fractions against temperature for the four C₅H₁₀O₂ isomers. It can be seen that, although BF, EP, and PA have very similar conversions, the formation of water and carbon dioxide differs from one to another isomers, propyl acetate being the isomer for which the formation of both of these final products occurs at the highest temperature. Indeed, while PA is consumed between 750–950 K, almost no H₂O and CO₂ formation is observed in this temperature range. The accumulation of both of these products starts above 950 K for PA (an explanation for this peculiar behavior is provided further in the discussion). Thus, whereas MB conversion starts ca. 890 K, it is immediately accompanied by water and CO₂ formation, the accumulation of these products appearing at a temperature lower than for PA. Another interesting point to notice is the evolution of the concentration of H₂O and CO₂ in the case of butyl formate. As can be seen in Fig. 4, the accumulation of both of these products is very similar for BF and EP in the temperature range 800–950 K. When T > 950 K, while H₂O and CO₂ mole fractions remain constant until ca. 1010 K in the case of BF, they keep increasing in the case of EP. In order to understand this behavior, the proposed kinetic mechanism was used to model the oxidation of mixtures of 1000 ppm of 1-butene and 1000 ppm of formic acid, 1000 ppm of propene and 1000 ppm of acetic acid, and 1000 ppm of ethylene and 1000 ppm of propanoic acid. The aim was to compare the oxidation of these mixtures, obtained if they were exclusively converted through their respective molecular reaction, with their respective ester.

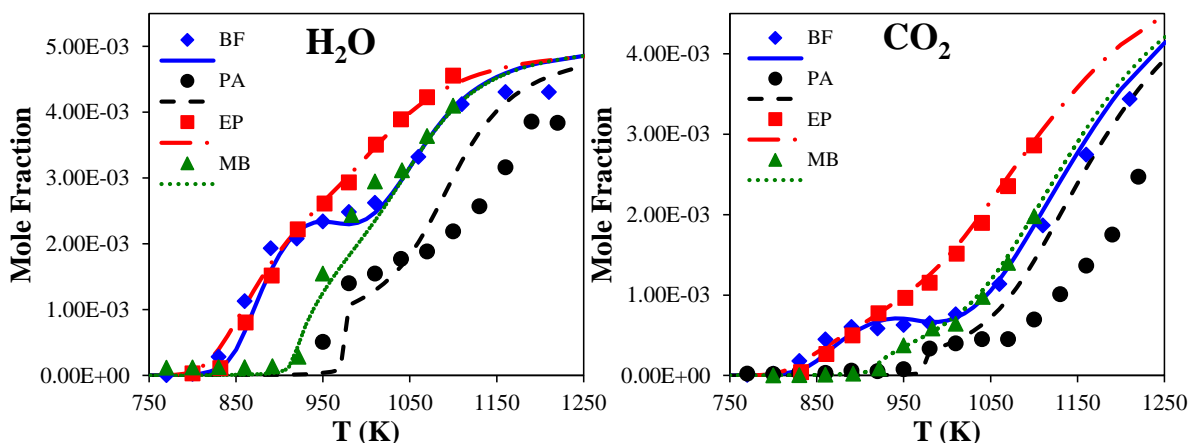


Figure 4: Experimental (large symbols) and computed (lines) mole fraction profiles of H_2O (left) and CO_2 (right) obtained from the oxidation of butyl formate (blue), propyl acetate (black), ethyl propanoate (red), and methyl butanoate (green), in a JSR at $\phi = 1$, $p = 10$ atm, $\tau = 0.7$ s.

Figure 5 presents the comparison between the computed water mole fraction profiles obtained from the oxidation of propyl acetate and $\text{C}_3\text{H}_6/\text{CH}_3\text{COOH}$ mixture (a), ethyl propanoate and $\text{C}_2\text{H}_4/\text{C}_2\text{H}_5\text{COOH}$ mixture (b), butyl formate and $\text{C}_4\text{H}_8\text{-1}/\text{HCOOH}$ mixture (c), in a JSR at $\phi = 1$, $p = 10$ atm, $\tau = 0.7$ s. Whereas the mixtures reproduce faithfully their respective ester oxidation for PA (a) and EP (b), the figure 5 c shows that $\text{C}_4\text{H}_8\text{-1}/\text{HCOOH}$ mixture is not able to reproduce the oxidation of BF between 850–1000 K. This means that in this temperature range, the accumulation of 1-butene and formic acid, which are produced by the fuel from 750 K, partly inhibits the reactivity until ca. 1000 K, temperature at which they start to significantly react and generate their own radical pool. Below 1000 K, while butyl formate partly decomposes into 1-butene and formic acid (40 % at 870 K as already mentioned in the previous section), the rest of BF reacts through H-abstraction reactions and increases the radical pool. At ca. 950 K, the concentration of almost unreactive $\text{C}_4\text{H}_8\text{-1}$ and HCOOH becomes too high, and they massively consume the small radicals produced by the radicals of

the fuel: the mole fraction of water (or CO_2) stagnates, or even slightly decreases. This behavior is between the two extremes: on one hand, the mixture of ethylene and propanoic acid from EP generates itself enough radicals to prevent the reactivity to decrease because of the accumulation of the products of the molecular decomposition (Fig. 5b), and, on the other hand, the mixture of propene and acetic acid completely inhibits branching reactions from propyl acetate, water starting to be produced in both cases only when the mixture $\text{C}_3\text{H}_6/\text{CH}_3\text{COOH}$ starts to react (Fig. 5a). Propyl acetate is only consumed by the molecular reaction.

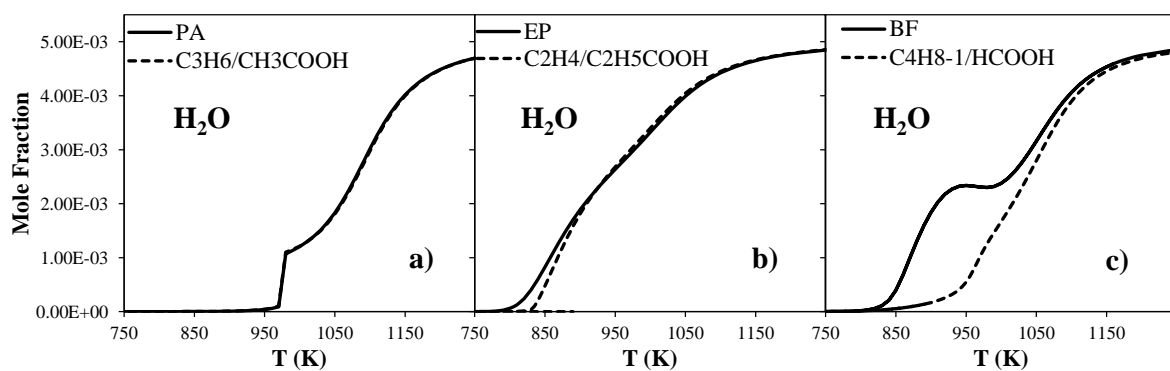


Figure 5: Comparison of computed water mole fraction profiles obtained from the oxidation of a) butyl formate (full line) and $\text{C}_4\text{H}_8-1/\text{HCOOH}$ mixture (dashed line), b) propyl acetate (full line) and $\text{C}_3\text{H}_6/\text{CH}_3\text{COOH}$ mixture (dashed line), c) ethyl propanoate (full line) and $\text{C}_2\text{H}_4/\text{C}_2\text{H}_5\text{COOH}$ mixture (dashed line), in a JSR at $\phi = 1$, $p = 10$ atm, $\tau = 0.7$ s.

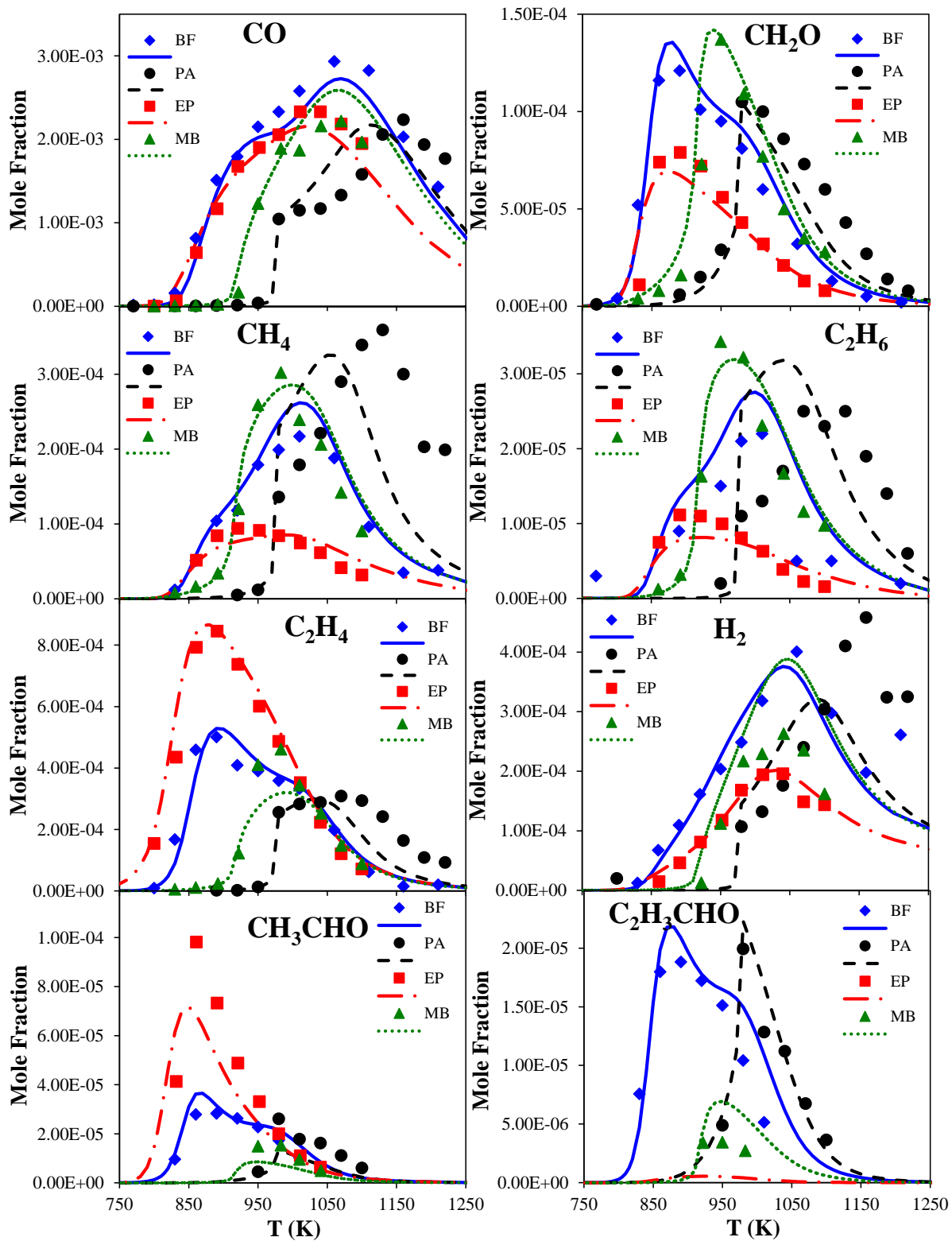


Figure 6: Comparison of experimental (symbols) and computed (lines) mole fraction profiles of some intermediates obtained from the oxidation of butyl formate (blue), propyl acetate

(black), ethyl propanoate (red), and methyl butanoate (green) in a JSR at $\phi = 1$, $p = 10$ atm, $\tau = 0.7$ s.

Figure 6 shows that similar conclusions could be made from the accumulation of other intermediates. All of these species presented in this figure start to accumulate at higher temperature in the case of propyl acetate than for any other isomers while intermediates start to accumulate at lower temperature for ethyl propanoate and butyl formate, with the case of methyl butanoate being in between. Generally speaking, BF produces slightly more CO than the other three. BF and MB also produce more formaldehyde, while EP produces less. EP yields less methane and ethane, indicating the formation of methyl radicals is limited with this isomer. It also produces less H₂ and acrolein while ethylene and acetaldehyde are abundantly produced, CH₃CHO being the product of the β -scission of a radical of EP.

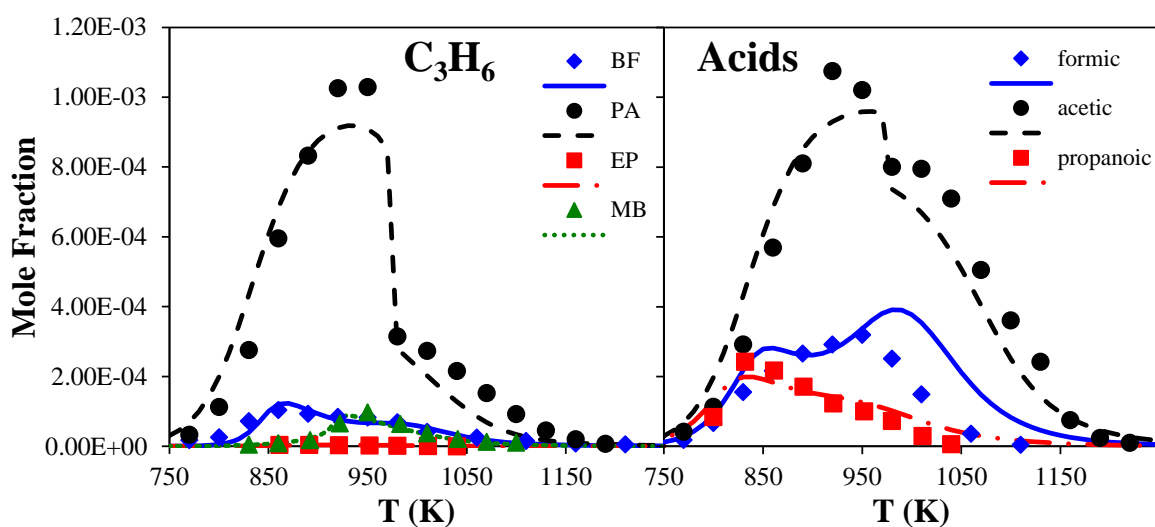


Figure 7: Comparison of experimental (symbols) and computed (lines) mole fraction profiles of C₃H₆ (left) and organic acids (right) obtained from the oxidation of butyl formate (blue), propyl acetate (black), ethyl propanoate (red), and methyl butanoate (green) in a JSR at $\phi = 1$, $p = 10$ atm, $\tau = 0.7$ s.

As an additional assessment of the role played by the products of the molecular decomposition reaction, the evolution of the mole fractions of propene (left) and three organic acids (right) are presented in Figure 7. From this figure it can be seen that propene accumulates up to ca. 1000 ppm (maximum mole fraction with 1000 ppm of PA) during the oxidation of propyl acetate whereas it hardly reaches 100 ppm when BF and MB are oxidized under the same conditions and only few ppm are produced from EP oxidation. This accumulation of propene, and the subsequent formation of the resonantly stabilized allyl radicals, is responsible for the gap in terms of temperature observed between the conversion of PA and the formation of water. Between 750 and 950 K, the radical pool is virtually inexistent, allowing acetic acid to accumulate up to 1000 ppm while PA is converted. The conversion of BF and EP is very similar to that of PA, but there, a radical pool is involved, making the rate of production of their respective acids (formic acid for BF and propanoic acid for EP) smaller and the rate of consumption of these acids higher than in the case of PA. Thus, acids accumulate less for BF and EP than for PA.

Finally, even though its influence may vary from one isomer to another, the radical pool is involved in the reactivity of these esters as detailed in the previous sections. Figure 8 presents the sum of the rates of production of H, O, OH, HO₂, and CH₃ as a function of the temperature for the four isomers. At 870 K, the radical pool participates to the consumption of EP and BF, EP being slightly more reactive with a higher radical concentration. The concentration of the radical pool is very low in the case of MB, making MB very little consumed, and extremely low in the case of PA allowing virtually no reactivity for C₃H₆ and acetic acid (the products of the molecular decomposition reaction). At 980 K, the radical pool concentration suddenly increases for PA, consuming massively C₃H₆ and acetic acid.

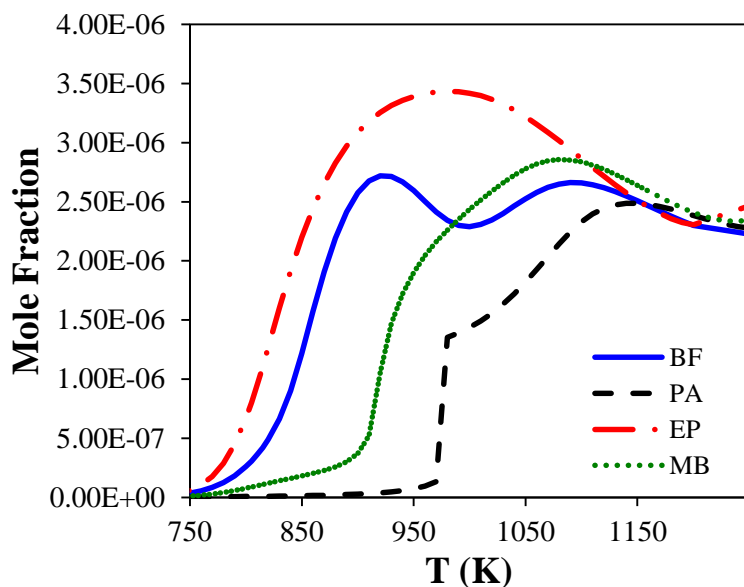


Figure 8: Sum of the computed mole fraction profiles of H, O, OH, HO₂ and CH₃ as a function of the temperature obtained from the oxidation of butyl formate (blue), propyl acetate (black), ethyl propanoate (red), and methyl butanoate (green) in a JSR at $\phi = 1$, $p = 10$ atm, $\tau = 0.7$ s.

5. Conclusion

In this study, the oxidation of four C₅H₁₀O₂ esters, namely butyl formate, propyl acetate, ethyl propanoate, and methyl butanoate, was experimentally studied in a jet-stirred reactor at $\phi = 1$, $p = 10$ atm, $\tau = 0.7$ s. The detailed kinetic mechanism developed in this work is well able to capture the experimental trends. This comparative study aims at demonstrating how the position of the ester function modifies not only the consumption of the fuel, but also the distribution of the products and the temperature at which they are formed. In particular, the six-membered ring transition state molecular reaction was found decisive to explain why butyl formate, propyl acetate, and ethyl propanoate are consumed very similarly while methyl butanoate starts to react at higher temperature. It was also observed that, the temperature at which intermediate compounds start to accumulate is higher for propyl acetate than for butyl formate, and ethyl propanoate, despite their similar consumption. This difference was found to lie in the capability of the products of the molecular decomposition reaction to generate their

own radical pool at a given temperature. Thus, it has been shown that the production of propene and acetic acid from propyl acetate completely inhibits the formation of radicals below 950 K, whereas the production of 1-butene and formic acid partly inhibits branching reactions, and the production of ethylene and propanoic acid is able to generate enough radicals to maintain the conversion of ethyl propanoate. The most efficient branching steps were shown to go through the oxidation of ethyl radicals, these radicals being partly regenerated by the addition of H atoms onto ethylene. It would be of interest to obtain experimental data in plug-flow reactors, shock tube or rapid compression machine in order to further strengthen these conclusions under broader conditions.

Acknowledgements

The research leading to these results has received funding from the European Research Council under the European Community's Seventh Framework Program (FP7/2007-2013) / ERC grant agreement n° 291049 – 2G-CSafe.

Supporting information: Kinetic mechanism and associated thermochemistry used here in CHEMKIN format.

List of figures

Figure 1: Experimental (large symbols) and computed (lines) mole fraction profiles obtained from the oxidation of methyl butanoate (green), ethyl propanoate (red), propyl acetate (black), and butyl formate (blue) in a JSR at $\varphi = 1$, $p = 10$ atm, $\tau = 0.7$ s.

Figure 2: Rate constants of the molecular reactions for ethyl propanoate (EP), butyl formate (BF), and propyl acetate (PA).

Figure 3: Rates of consumption and formation of C_2H_5 calculated at $T = 870$ K, $p = 10$ atm, $\varphi = 1$, and $\tau = 0.7$ s for a) ethyl propanoate (EP), b) butyl formate (BF), c) methyl butanoate (MB), and d) propyl acetate (PA).

Figure 4: Experimental (large symbols) and computed (lines) mole fraction profiles of H_2O (left) and CO_2 (right) obtained from the oxidation of butyl formate (blue), propyl acetate (black), ethyl propanoate (red), and methyl butanoate (green), in a JSR at $\varphi = 1$, $p = 10$ atm, $\tau = 0.7$ s.

Figure 5: Comparison of computed water mole fraction profiles obtained from the oxidation of a) butyl formate (full line) and $C_4H_8-1/HCOOH$ mixture (dashed line), b) propyl acetate (full line) and C_3H_6/CH_3COOH mixture (dashed line), c) ethyl propanoate (full line) and C_2H_4/C_2H_5COOH mixture (dashed line), in a JSR at $\varphi = 1$, $p = 10$ atm, $\tau = 0.7$ s.

Figure 6: Comparison of experimental (symbols) and computed (lines) mole fraction profiles of some intermediates obtained from the oxidation of butyl formate (blue), propyl acetate (black), ethyl propanoate (red), and methyl butanoate (green) in a JSR at $\varphi = 1$, $p = 10$ atm, $\tau = 0.7$ s.

Figure 7: Comparison of experimental (symbols) and computed (lines) mole fraction profiles of C_3H_6 (left) and organic acids (right) obtained from the oxidation of butyl formate (blue), propyl acetate (black), ethyl propanoate (red), and methyl butanoate (green) in a JSR at $\varphi = 1$, $p = 10$ atm, $\tau = 0.7$ s.

Figure 8: Sum of the computed mole fraction profiles of H, O, OH, HO_2 and CH_3 as a function of the temperature obtained from the oxidation of butyl formate (blue), propyl acetate (black), ethyl propanoate (red), and methyl butanoate (green) in a JSR at $\varphi = 1$, $p = 10$ atm, $\tau = 0.7$ s.

References

1. Dagaut, P.; Smoucovit, N.; Cathonnet, M. Methyl Acetate Oxidation in a JSR: Experimental and Detailed Kinetic Modeling Study, *Combustion Science and Technology* 1997, 127, 275-291.
2. Fisher, E. M.; Pitz, W. J.; Curran, H. J.; Westbrook, C. K. Detailed chemical kinetic mechanisms for combustion of oxygenated fuels, *Proceedings of the Combustion Institute* 2000, 28, 1579-1586.
3. Herbinet, O.; Pitz, W. J.; Westbrook, C. K. Detailed chemical kinetic oxidation mechanism for a biodiesel surrogate, *Combustion and Flame* 2008, 154, 507-528.
4. Zhang, K. W.; Togbe, C.; Dayma, G.; Dagaut, P. Experimental and kinetic modeling study of trans-methyl-3-hexenoate oxidation in JSR and the role of C=C double bond, *Combustion and Flame* 2014, 161, 818-825.
5. Gerasimov, I. E.; Knyazkov, D. A.; Bolshova, T. A.; Shmakov, A. G.; Korobeinichev, O. P.; Carbonnier, M.; Lefort, B.; Kéromnès, A.; Le Moyne, L.; Lubrano Lavadera, M.; Konnov, A. A.; Zhou, C.-W.; Serinyel, Z.; Dayma, G.; Dagaut, P. Methyl-3-hexenoate combustion chemistry: Experimental study and numerical kinetic simulation, *Combustion and Flame* 2020, 222, 170-180.
6. Dayma, G.; Halter, F.; Foucher, F.; Togbé, C.; Mounaim-Rousselle, C.; Dagaut, P. Experimental and Detailed Kinetic Modeling Study of Ethyl Pentanoate (Ethyl Valerate) Oxidation in a Jet Stirred Reactor and Laminar Burning Velocities in a Spherical Combustion Chamber, *Energy & Fuels* 2012, 26, 4735-4748.
7. Zaras, A. M.; Szóri, M.; Thion, S.; Van Cauwenberghe, P.; Deguillaume, F.; Serinyel, Z.; Dayma, G.; Dagaut, P. A Chemical Kinetic Investigation on Butyl Formate Oxidation: Ab Initio Calculations and Experiments in a Jet-Stirred Reactor, *Energy & Fuels* 2017, 31, 6194-6205.
8. Togbé, C.; Dagaut, P.; Mzé-Ahmed, A.; Diévar, P.; Halter, F.; Foucher, F. Experimental and Detailed Kinetic Modeling Study of 1-Hexanol Oxidation in a Pressurized Jet-Stirred Reactor and a Combustion Bomb, *Energy & Fuels* 2010, 24, 5859-5875.
9. Carbonnier, M.; Serinyel, Z.; Kéromnès, A.; Dayma, G.; Lefort, B.; Le Moyne, L.; Dagaut, P. An experimental and modeling study of the oxidation of 3-pentanol at high pressure, *Proceedings of the Combustion Institute* 2018, 37, 477-484.
10. Serinyel, Z.; Togbé, C.; Dayma, G.; Dagaut, P. An experimental and modeling study of 2-methyl-1-butanol oxidation in a jet-stirred reactor, *Combustion and Flame* 2014, 161, 3003-3013.
11. Dayma, G.; Togbé, C.; Dagaut, P. Experimental and Detailed Kinetic Modeling Study of Isoamyl Alcohol (Isopentanol) Oxidation in a Jet-Stirred Reactor at Elevated Pressure, *Energy & Fuels* 2011, 25, 4986-4998.
12. Bai, J.; Zhu, Y.; Zhou, C.-W.; Dayma, G.; Serinyel, Z.; Dagaut, P. Oxidation of pentan-2-ol – Part I: Theoretical investigation on the decomposition and isomerization reactions of pentan-2-ol radicals, *Proceedings of the Combustion Institute* 2021, 38, 823-832.
13. Dayma, G.; Serinyel, Z.; Carbonnier, M.; Bai, J.; Zhu, Y.; Zhou, C.-W.; Kéromnès, A.; Lefort, B.; Le Moyne, L.; Dagaut, P. Oxidation of pentan-2-ol – part II: Experimental and modeling study, *Proceedings of the Combustion Institute* 2021, 38, 833-841.
14. Contino, F.; Dagaut, P.; Dayma, G.; Halter, F.; Foucher, F.; Mounaim-Rousselle, C. Combustion and Emissions Characteristics of Valeric Biofuels in a Compression Ignition Engine, *Journal of Energy Engineering* 2014, 140, A4014013-A4014013.
15. Contino, F.; Dagaut, P.; Halter, F.; Masurier, J.-B.; Dayma, G.; Mounaim-Rousselle, C.; Foucher, F. Screening Method for Fuels in Homogeneous Charge Compression Ignition Engines: Application to Valeric Biofuels, *Energy & Fuels* 2017, 31, 607-614.
16. Metcalfe, W. K.; Togbé, C.; Dagaut, P.; Curran, H. J.; Simmie, J. M. A jet-stirred reactor and kinetic modeling study of ethyl propanoate oxidation, *Combustion and Flame* 2009, 156, 250-260.
17. Dayma, G.; Thion, S.; Lailliau, M.; Serinyel, Z.; Dagaut, P.; Sirjean, B.; Fournet, R. Kinetics of propyl acetate oxidation: Experiments in a jet-stirred reactor, ab initio calculations, and rate constant determination, *Proceedings of the Combustion Institute* 2019, 37, 429-436.
18. Gail, S.; Thomson, M. J.; Sarathy, S. M.; Syed, S. A.; Dagaut, P.; Diévar, P.; Marchese, A. J.; Dryer, F. L. A wide-ranging kinetic modeling study of methyl butanoate combustion, *Proceedings of the Combustion Institute* 2007, 31 I, 305-311.
19. Ramirez, H. P.; Hadj-Ali, K.; Diévar, P.; Dayma, G.; Togbé, C.; Moréac, G.; Dagaut, P. Oxidation of commercial and surrogate bio-Diesel fuels (B30) in a jet-stirred reactor at elevated pressure: Experimental and modeling kinetic study, *Proceedings of the Combustion Institute* 2011, 33, 375-382.
20. Mzé-Ahmed, A.; Dagaut, P.; Hadj-Ali, K.; Dayma, G.; Kick, T.; Herbst, J.; Kathrotia, T.; Braun-Unkhoff, M.; Herzler, J.; Naumann, C.; Riedel, U. Oxidation of a Coal-to-Liquid Synthetic Jet Fuel: Experimental and Chemical Kinetic Modeling Study, *Energy & Fuels* 2012, 26, 6070-6079.
21. Glarborg, P.; Kee, R. J.; Grcar, J. F.; Miller, J. A.; Sandia National Laboratories, Livermore, CA (USA), 1986.

22. Fenard, Y.; Dagaut, P.; Dayma, G.; Halter, F.; Foucher, F. Experimental and kinetic modeling study of trans-2-butene oxidation in a jet-stirred reactor and a combustion bomb, *Proceedings of the Combustion Institute* 2015, 35, 317-324.
23. Fenard, Y.; Dayma, G.; Halter, F.; Foucher, F.; Serinyel, Z.; Dagaut, P. Experimental and Modeling Study of the Oxidation of 1-Butene and cis-2-Butene in a Jet-Stirred Reactor and a Combustion Vessel, *Energy & Fuels* 2015, 29, 1107-1118.
24. El-Nahas, A. M.; Navarro, M. V.; Simmie, J. M.; Bozzelli, J. W.; Curran, H. J.; Dooley, S.; Metcalfe, W. Enthalpies of formation, bond dissociation energies and reaction paths for the decomposition of model biofuels: Ethyl propanoate and methyl butanoate, *Journal of Physical Chemistry A* 2007, 111, 3727-3739.
25. Dayma, G.; Halter, F.; Foucher, F.; Mounaim-Rousselle, C.; Dagaut, P. Laminar Burning Velocities of C4-C7 Ethyl Esters in a Spherical Combustion Chamber: Experimental and Detailed Kinetic Modeling, *Energy & Fuels* 2012, 26, 6669-6677.